Modeling, Analysis, and Identification of Armature Winding Interturn Fault in Multiphase Brushless Exciters

Liangliang Hao, *Member, IEEE*, Jianlin Chen, *Student Member, IEEE*, Li He, Xianwen Duan, Peng He, and Guang Wang

***Abstract*—As the core of large-capacity nuclear power generation system, the multiphase annular brushless exciter (MPABE) may cause a serious catastrophe to the nuclear power plant if it fails. In order to effectively protect the armature winding of MPABE, a rapid simulation model and a sensitive diagnosis method of armature winding short-circuit (AWSC) fault are studied systematically in this article. First, this article proposes a general and rapid simulation model of MPABE with AWSC fault. To verify the correctness of this model, corresponding simulations and experiments of AWSC faults are carried out, respectively, through which the fault characteristics are obtained. Then, a detailed mechanism analysis is presented, which explains the induction process of the related harmonics in the stator and rotor currents. The variation law of the characteristics value when the number of short-circuited coils changes is also analyzed. Finally, a new method to diagnose AWSC fault of the MPABE is proposed and then optimized. The test results on the prototype show that this method can sensitively diagnose even the slightest AWSC fault. Therefore, it can provide a reliable basis for the monitoring and protection of MPABE in nuclear power plants.**

***Index Terms*—Armature winding short-circuits (AWSC), fault diagnosis, harmonic characteristics, multiphase annular brushless exciter (MPABE), rapid simulation model.**

I. Introduction

NUCLEAR power, which is efficient and pollution-free, has gradually become the preferred energy for power generation. However, with the increasing capacity of a single nuclear power generator, the safety and reliability of nuclear power plant operation is receiving more and more attention [1].

Excitation system is an important part of large generation sets in a nuclear power plant [2], [3]. Compared with the static excitation system, brushless excitation cancels the carbon brushes and collector rings, significantly improves the reliability of the excitation system [4], [5], and has become a mainstream excitation mode of large-capacity nuclear power units. In particular, a kind of MPABE system has appeared in recent years, which is widely used in large-capacity nuclear power units such as Hongyanhe, Ningde, Taishan, and other power plants in China.

The structure of the MPABE system is shown in Fig. 1(e.g., *m*-phase annular brushless exciter), which is a two-machine (exciter-generator) brushless excitation system. The MPABE is actually a salient-pole synchronous machine with rotating-armature structure, where the field winding is internal and on the stator, while the armature windings are external and on the rotor. Unlike other machines, an annular structure with end-to-end connection is adopted in the MPABE armature windings, which rotate at high speed together with the multiphase rectifier bridge composed of diodes. The output dc voltage is supplied to the excitation winding of the main generator. To prevent diode overcurrent burnout, fuses are also provided between the armature winding of the exciter and the rectifier.

During normal operation, the whole rectifier system rotates at high speed, which makes armature winding and diode very prone to failure. The following three faults often occur and are

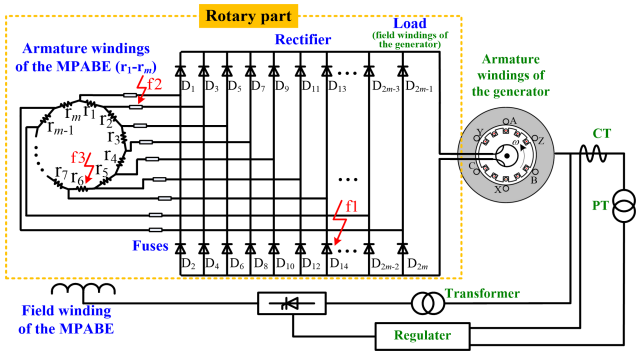

Fig. 1. *m*-phase annular brushless exciter with a rotary rectifier.

Manuscript received 11 February 2022; revised 10 July 2022; accepted 12 August 2022. Date of publication 22 August 2022; date of current version 10 October 2022. This work was supported in part by the Fundamental Research Funds for the Central Universities under Grant 2021YJS153 and Grant 2020JBM070 and in part by the Scientific and Technological Project of China Nuclear Power Operation Co., Ltd. (Research and Implementation of Fault Characteristic Analysis and Relay Protection Configuration of Brushless Exciter for Million-kilowatt Nuclear Power Units). Recommended for publication by Associate Editor E. Armando. *(Corresponding author: Liangliang Hao.)*

Liangliang Hao and Jianlin Chen are with the School of Electrical Engineering, Beijing Jiaotong University, Beijing 100044, China (e-mail: haoll07@mails.tsinghua.edu.cn; 20117018@bjtu.edu.cn).

Li He is with the Yangjiang Nuclear Power Company, Ltd., Yangjiang 529500, China (e-mail: heli@cgnpc.com.cn).

Xianwen Duan is with the China Nuclear Power Operations Company, Ltd., Shenzhen 440304, China (e-mail: 952102547@qq.com).

Peng He is with the Liaoning Hongyanhe Nuclear Power Company, Ltd., Dalian 116302, China (e-mail: hepeng2@cgnpc.com.cn).

Guang Wang is with the Nanjing NR Electric Company, Ltd., Nanjing 211102, China (e-mail: wangg@nrec.com).

Color versions of one or more figures in this article are available at https://doi.org/10.1109/TPEL.2022.3200675.

Digital Object Identifier 10.1109/TPEL.2022.3200675

concerned in engineering practice: rectifier open-circuit fault (f1), fuse open-circuit fault (f2), and armature winding short-circuit fault (f3). In the case of winding short-circuit faults, the fault currents will increase to tens or even dozens of times of the rated current, resulting in overheating and burning of armature windings in a short time, which seriously endangers the safe operation of exciter and power generation system. Nevertheless, at present, the MPABE system still operates in a "weak protection" state. Generally, it is only equipped with some simple overcurrent protection, but there is no corresponding protection or monitoring devices for the internal faults of stator and rotor. In recent years, there have been many serious incidents caused by the exciter fault, resulting in huge losses. For example, in December 2017, a short-circuit fault occurred in the rotor armature winding of the exciter in Zhejiang Yuhuan Power Plant #4 unit. Since there was no exciter protection, the fault continued until the rotor vibration exceeded the standard and trips. The accident analysis after the event showed that 10 (30 in total) conducting copper bars from the exciter rotor armature winding to the rectifier were blown due to the short-circuit fault. More unfortunately, the exciter rotor winding was burned beyond recognition and completely scrapped. Therefore, it is urgent to effectively diagnose the AWSC fault of the MPABE.

Lots of research has been carried out on the AWSC fault, which mainly focuses on the following two aspects.

1) *Fault characteristics:* Mainly including the characteristics of three-phase synchronous generator [6], [7], [8], induction motor [9], [10], [11], doubly fed induction motor [12], [13], and permanent magnet motor [14], [15], [16], [17]. Although the types of motors are different, the proposed fault diagnosis methods are similar. There are mainly diagnosis methods characterized by stator or rotor current harmonic characteristics [7], [8], [10], [15], [17], stator current sequence component [9], [13], [16], and air gap magnetic flux [11], [12] MPABE system, which plays an increasingly important role in a nuclear power plant, is essentially synchronous generator with rectifier system. There is also some literature on the internal faults of this kind of motor with rectifier system. In [18] and [19], the AWSC of three-phase and five-phase star motor with rectifier in automotive power system is analyzed. In [20] and [21], the AWSC fault of a 12-phase motor with rectifier system is simulated and experimentally studied. However, the 12-phase rectifier system of the motor is actually composed of four independent three-phase rectifier bridges.
2) *Fault simulation model:* As an effective method to study the fault of induction motor, finite element (FEM) simulation calculation is now commonly used [23], [24]. However, because it takes into account both cogging effect and saturation effect, which are difficult to calculate, the calculation speed is very slow. It takes 20 h or even longer to calculate a complete AWSC fault [25](inter(R) Core (TM) i7-4790K CPU @4.00 GHz and 16.0 GB RAM), which has always been a difficult problem for many researchers. At present, the methods for rapid simulation modeling of synchronous generator with rectifier system include pattern classification method [26], tensor method [4], and multiloop method [27], [28], [29], [30], which can provide some experience for this article.

Based on the abovementioned observations, we note that great progress has been made in the research of fault characteristics and simulation models. However, what has been achieved may not be well applied to MPABEs, for there are still some limitations.

1) The commutation process and actual conduction of the rectifier system in MPABE are more complex, which increases the research difficulty. Moreover, MPABE's special rotating-armature structure and annular winding connection are completely different from those of a star motor. Therefore, the AWSC fault analysis and diagnosis method are quite different from those of the abovementioned motor types. In addition, due to the large excitation power of MPABE, any degree of short-circuit fault may cause serious damage to the exciter. However, at present, there is no sensitive diagnostic method that can achieve 100% protection.
2) Fault diagnosis through the stator excitation current is a feasible and effective method [22]. However, since the short-circuit current in the armature winding passes through the transition and conversion of the air gap magnetic field, rather than directly transmitted to the excitation winding, the final characteristic performance in excitation winding under fault becomes unclear. Furthermore, when the number of short-circuited armature winding coils changes, the variation law of fault characteristic value becomes different. In this article, it is found that the more short-circuited coils there are in a certain range, the smaller the fault characteristic value is, sometimes even smaller than that of 1-coil AWSC fault, resulting in insufficient protection sensitivity, which makes it unlikely to identify the fault. However, up to now, there has been a lack of systematic research on fault characteristic and its variation law of AWSC in MPABE.
3) In this article, the faults with various coils need to be calculated for many times. Besides, it takes a long time for the AWSC fault to change from the fault moment to the postfault steady state. Therefore, the FEM is not feasible for the AWSC fault simulation of MPABE because of the huge amounts of computation and long time spent. Similarly, two other simulation methods are not quite feasible: the pattern classification method needs to make a deeper analysis of the diode commutation process, and the tensor method needs to introduce the intermediate network for two transformations. The programming of both of them is more difficult and complex. Therefore, a simpler and more efficient rapid simulation method is needed.

By contrast, the multiloop method can automatically generate the correlation transformation matrix, which describes the dynamic connection relationship of each element in the network and the actual loop according to the diode commutation process and conduction. Only one network transformation is needed in the calculation, which greatly shortens the simulation time.

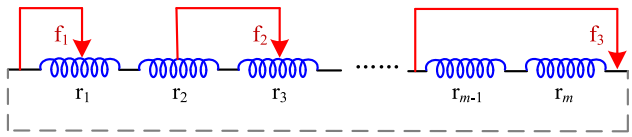

Fig. 2. Rotor armature windings short-circuit faults.

Therefore, the multiloop method can be applied to modeling the MPABE with an AWSC fault.

Driven by the abovementioned three restrictions, this article studies a novel rapid simulation model, fault characteristics, and a sensitive diagnosis method of AWSC fault in MPABE. The main contributions of this article can be summarized as follows.

1) A rapid simulation method for general MPABEs is proposed. It takes only about fifteen minutes for the model to complete the calculation of a fault, and the accuracy of the model has been verified by the prototype experiments.
2) A theoretical analysis of AWSC fault characteristics spectrum and its variation law is presented for the first time. The analytical method and conclusion can be extended to MPABE with other phase numbers.
3) A complete and sensitive diagnosis method for 100% protection of armature winding is proposed. This protection method can sensitively diagnose AWSC faults at any position and at any time.

The rest of this article is organized as follows. Section II illustrates the actual connection of stator and rotor winding of MPABE and constructs the rapid simulation model. Section III verifies the proposed rapid simulation model via experimental results. In Section IV, the AWSC fault characteristics and their variation law with different number of short-circuited coils are comprehensively analyzed. Section V presents the fault diagnosis method for AWSC fault. Finally, Section VI concludes this article.

II. Rapid Simulation Mathematical Model

A. Voltage Equations of Rotor and Stator Windings

This article assumes that the generator routine is adopted in the rotor loops, where the positive directions of the loop voltage and loop current are the same when observed in the direction of load; and that the motor routine is adopted in the stator loop, where the positive directions of the loop voltage and loop current are the same when observed in the direction of winding. Meanwhile, positive stator and rotor currents are required to produce positive flux linkage.

1). Voltage Equation of Rotor Armature Windings: In the normal operation, each phase of rotor armature windings is regarded as one branch. As shown in Fig. 2, when an AWSC fault occurs, the faulty winding is divided into two branches from the short-circuit point (excluding the short-circuit fault at terminal). In this article, the considered faults are the in-phase short-circuit fault (f1) and the interphase short-circuit fault at nonterminal (f2) or at terminal (f3).

The total number of rotor branches varies with the types of the AWSC fault, which can be defined as follows:

$$N=\begin{cases} m, & \text{normal operation} \\ & \text{(or inter-phase short-circuit fault at terminal)} \\ m+1, & \text{in-phase short-circuit fault} \\ m{+}2, & \text{inter-phase short-circuit fault at nonterminal} \end{cases} \tag{1}$$

where m is the phase number of the MPABE.

The voltage equation in the rotor armature winding can be written as

$$\begin{bmatrix} u_{\mathrm{r}1} \\ u_{\mathrm{r}2} \\ \vdots \\ u_{\mathrm{r}N} \end{bmatrix} = p \begin{bmatrix} \psi_{\mathrm{r}1} \\ \psi_{\mathrm{r}2} \\ \vdots \\ \psi_{\mathrm{r}N} \end{bmatrix} - \begin{bmatrix} r_{\mathrm{r}1} & 0 & \cdots & 0 \\ 0 & r_{\mathrm{r}2} & \cdots & 0 \\ \vdots & \vdots & \ddots & \vdots \\ 0 & 0 & \cdots & r_{\mathrm{r}N} \end{bmatrix} \begin{bmatrix} i_{\mathrm{r}1} \\ i_{\mathrm{r}2} \\ \vdots \\ i_{\mathrm{r}N} \end{bmatrix} \tag{2}$$

where $u_{\mathrm{r}i}$, $\psi_{\mathrm{r}i}$, $r_{\mathrm{r}i}$, $i_{\mathrm{r}i}$ are the voltage, flux, resistance, and current of the ith branch in the rotor, respectively, and p is the differential operator d/dt.

Each branch in the rotor (including faulty armature branch) and the stator field winding contribute to the flux of the ith branch in the rotor, which can be expressed as

$$\begin{aligned} \psi_{\mathrm{r}i} &= \left[\begin{array}{c|ccc} M_{\mathrm{r}1,\mathrm{fd}} & L_{\mathrm{r}1} & M_{\mathrm{r}1,\mathrm{r}2} & \cdots & M_{\mathrm{r}1,\mathrm{r}N} \\ M_{\mathrm{r}2,\mathrm{fd}} & M_{\mathrm{r}2,\mathrm{r}1} & L_{\mathrm{r}2} & \cdots & M_{\mathrm{r}2,\mathrm{r}N} \\ \vdots & \vdots & \vdots & \ddots & \vdots \\ M_{\mathrm{r}N,\mathrm{fd}} & M_{\mathrm{r}N,\mathrm{r}1} & M_{\mathrm{r}N,\mathrm{r}2} & \cdots & L_{\mathrm{r}N} \end{array}\right] \begin{bmatrix} i_{\mathrm{fd}} \\ i_{\mathrm{r}1} \\ i_{\mathrm{r}2} \\ \vdots \\ i_{\mathrm{r}N} \end{bmatrix} \\ &= M_{\mathrm{r}i,\mathrm{fd}} i_{\mathrm{fd}} + \sum_{j=1}^{N} M_{\mathrm{r}i,\mathrm{r}j} i_{\mathrm{r}j} \end{aligned} \tag{3}$$

where $M_{\mathrm{r}i,\mathrm{fd}}$ is the mutual inductance between the ith branch in the rotor and the field winding, i_{fd} is the field current, and $M_{\mathrm{r}i,\mathrm{r}j}$ is the mutual inductance between the ith branch and the jth branch in the rotor.

By using (3) and (2), the voltage equation of the ith branch in the rotor with $i_{\mathrm{r}i}$, as an unknown can be written as

$$u_{\mathrm{r}i} = p\left(M_{\mathrm{r}i,\mathrm{fd}} i_{\mathrm{fd}} + \sum_{j=1}^{N} M_{\mathrm{r}i,\mathrm{r}j} i_{\mathrm{r}j}\right) - r_{\mathrm{r}i} i_{\mathrm{r}i}. \tag{4}$$

2) Voltage Equation of Stator Field Winding:

$$u_{\mathrm{fd}} = p\psi_{\mathrm{fd}} - r_{\mathrm{fd}} i_{\mathrm{fd}} \tag{5}$$

where u_{fd}, ψ_{fd}, $r_{\mathrm{fd}}$are the voltage, flux, and resistance of the field winding, respectively. Without considering the role of the excitation regulater, u_{fd} is a constant and remains unchanged after the fault.

Any branch of exciter, including faulty armature branch, contributes to the stator flux, which can be written as

$$\psi_{\mathrm{fd}} = \left[L_{\mathrm{fd}} | M_{\mathrm{r}1,\mathrm{fd}} \cdots \; M_{\mathrm{r}N,\mathrm{fd}}\right] \begin{bmatrix} i_{\mathrm{fd}} \\ i_{\mathrm{r}1} \\ i_{\mathrm{r}2} \\ \vdots \\ i_{\mathrm{r}N} \end{bmatrix}$$

$$= L_{\mathrm{fd}} i_{\mathrm{fd}} + \sum_{i=1}^{N} M_{\mathrm{r}i,\mathrm{fd}} i_{\mathrm{r}i} \tag{6}$$

where L_{fd} is the self-inductance of the field winding.

Used (5) and (6), the voltage equation of the field winding with i_{fd}, as an unknown can be written as

$$u_{\mathrm{fd}} = p\left(L_{\mathrm{fd}} i_{\mathrm{fd}} + \sum_{i=1}^{N} M_{\mathrm{r}i,\mathrm{fd}} i_{\mathrm{r}i}\right) + r_{\mathrm{fd}} i_{\mathrm{fd}}. \tag{7}$$

B. Voltage Equation of the DC Load

As can be seen in Fig. 1, the load of the MPABE is the field winding of the main generator, and its voltage equation is as

$$u_{\mathrm{dc}} - E_{\mathrm{dc}} = L_{\mathrm{dc}} \frac{\mathrm{d}i_{\mathrm{dc}}}{\mathrm{d}t} + R_{\mathrm{dc}} i_{\mathrm{dc}} \tag{8}$$

where u_{dc}, L_{dc}, R_{dc}, and E_{dc} are the voltage, inductance, resistance, and back electromotive force (EMF) of the load, respectively. Generally, the E_{dc} is equal to zero no matter in the normal operation or under the AWSC fault [25].

C. System Equation

By using the voltage equation of each branch mentioned previously, we can obtain the system equation as follows:

$$\begin{bmatrix} u_{\mathrm{fd}} \\ u_{\mathrm{r1}} \\ u_{\mathrm{r2}} \\ \vdots \\ u_{\mathrm{r}N} \\ u_{\mathrm{dc}} \end{bmatrix} = p\left(\left[\begin{array}{c|cccc|c} L_{\mathrm{fd}} & M_{\mathrm{r1,fd}} & M_{\mathrm{r2,fd}} & \cdots & M_{\mathrm{r}N,\mathrm{fd}} & 0 \\ \hline M_{\mathrm{r1,fd}} & L_{\mathrm{r1}} & M_{\mathrm{r1,r2}} & \cdots & M_{\mathrm{r1,r}N} & 0 \\ M_{\mathrm{r2,fd}} & M_{\mathrm{r2,r1}} & L_{\mathrm{r2}} & \cdots & M_{\mathrm{r2,r}N} & 0 \\ \vdots & \vdots & \vdots & \ddots & \vdots & \vdots \\ M_{\mathrm{r}N,\mathrm{fd}} & M_{\mathrm{r}N,\mathrm{r1}} & M_{\mathrm{r}N,\mathrm{r2}} & \cdots & L_{\mathrm{r}N} & 0 \\ \hline 0 & 0 & 0 & \cdots & 0 & L_{\mathrm{dc}} \end{array}\right] \begin{bmatrix} i_{\mathrm{fd}} \\ i_{\mathrm{r1}} \\ i_{\mathrm{r2}} \\ \vdots \\ i_{\mathrm{r}N} \\ i_{\mathrm{dc}} \end{bmatrix}\right) + \begin{bmatrix} r_{\mathrm{fd}} & & & & & \\ & -r_{\mathrm{r1}} & & & & \\ & & -r_{\mathrm{r2}} & & & \\ & & & \ddots & & \\ & & & & -r_{\mathrm{r}N} & \\ & & & & & r_{\mathrm{dc}} \end{bmatrix} \begin{bmatrix} i_{\mathrm{fd}} \\ i_{\mathrm{r1}} \\ i_{\mathrm{r2}} \\ \vdots \\ i_{\mathrm{r}N} \\ i_{\mathrm{dc}} \end{bmatrix} \tag{9}$$

Furthermore, (9) can be simplified to a matrix equation

$$\boldsymbol{U} = p(\boldsymbol{M}\boldsymbol{I}) + \boldsymbol{R}\boldsymbol{I} \tag{10}$$

where $\boldsymbol{U}$, $\boldsymbol{I}$, and $\boldsymbol{R}$ are the vectors of the voltage, current, and resistance of the MPABE, while $\boldsymbol{M}$ is the inductance matrix, respectively.

The MLM takes a coil as a basic unit to calculate the self and mutual inductances between the rotor and stator windings, considering all harmonics of the air-gap magnetic field. Specifically, the relevant formulas are given in [27].

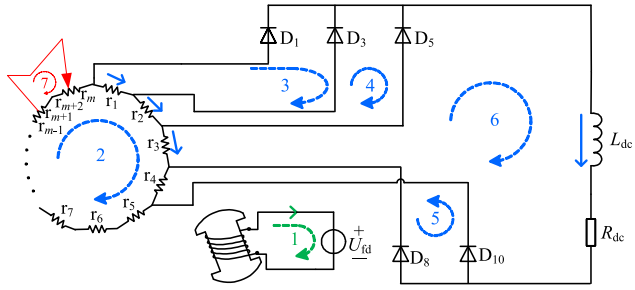

Fig. 3. Topology of the m-phase excitation system.

D. Actual Connection Between Rotor Windings and Load

1) Turn-on and Turn-off Criterion of the Diodes: The correct generation of the correlation transformation matrix $\boldsymbol{B}$ is the key of correct state equation and accurate simulation. However, the matrix $\boldsymbol{B}$ totally depends on the turn-ON and turn-OFF of the diodes, which are controlled by external circuits and also directly affect the topology of the system.

In this article, according to the actual physical conditions of the diodes, it is judged that when the voltage-drop between the two poles of a diode is positive, the diode will turn ON, that when the current of a diode changes from positive to negative, the diode will turn OFF. Specifically, the largest one is selected from all the line-voltages of the rectifier; when it is greater than the dc load voltage plus 2 times the diode voltage-drop, both of the corresponding diodes will turn ON; and when the current of a diode is less than zero, it will turn OFF.

2) Correlation Transformation Matrix: Actually, the rotor windings of the MPABE are connected to the load through a multiphase rectifier. The actual connection relationship between the windings and the load will change with the conduction process of the rectifier, which can be described by the correlation transformation matrix $\boldsymbol{B}$.

Each column in the matrix $\boldsymbol{B}$ corresponds to each branch, and the column number varies with different fault types. Each row corresponds to each loop, and the row number varies with the commutation of the rectifier diodes. It is provided that the matrix element is "1" when the loop and the branch are in the same reference directions, the matrix element is "-1" when they are in the opposite reference directions, and the matrix element is "0" when they are independent.

Due to the annular structure of the armature windings, the commutation process of the rectifier is complex and there are multiple (more than three) diodes conducting simultaneously. Assuming that the diodes D_1, D_3, D_5, D_8, and D_{10} turn ON at a certain moment, the rectifier is in a commutation state. The topology of the excitation system is shown in Fig. 3, where the reference directions of the branches and the loops are marked. As we can see, there are six independent loops in the normal operation: the first loop is formed by the stator winding, while the second loop to the sixth loop is formed by the rotor windings, the turned-ON diodes and the load. If there is an AWSC fault (e.g., the interphase short-circuit fault at nonterminal), an additional loop (i.e., the seventh loop) formed by the faulty rotor windings will be added to the system.

Each rotor winding (including the faulty windings), the stator winding and the load are considered as one branch respectively. According to Fig. 3, the correlation transformation matrix $\boldsymbol{B}$ can be written as

$$\boldsymbol{B} =$$

fd	r_1	r_2	r_3	r_4	r_5	$\cdots$	r_m	dc	r_{m+1}	r_{m+2}	
1	0	0	0	0	0	...	0	0	0	0	loop1
0	1	1	1	1	1	...	1	0	0	0	loop2
0	−1	0	0	0	0	...	0	0	0	0	loop3
0	0	−1	0	0	0	...	0	0	0	0	loop4
0	0	0	−1	0	0	...	0	0	0	0	loop5
0	0	0	0	−1	0	...	0	1	0	0	loop6
0	0	0	0	0	0	...	0	0	−1	−1	loop7

where "fd" stands for the field winding, "r_1"-"r_m" stand for the healthy armature windings of Phase 1 to Phase m, respectively, "dc" stands for the dc load, and "r_{m+1}"-"r_{m+2}" stand for faulty armature windings of Phase m-1 and Phase m, respectively.

Similarly, referring to the abovementioned process, the matrix $\boldsymbol{B}$ can also be derived when the AWSC faults occur at other positions.

3) Standard State Equation: The matrix $\boldsymbol{B}$ is used, and then

$$\boldsymbol{U}' = \boldsymbol{BU} \tag{11}$$

$$\boldsymbol{B}^{\mathrm{T}}\boldsymbol{I}' = \boldsymbol{I}. \tag{12}$$

By using (11) and (12), (10) can be changed into

$$p\boldsymbol{I}' = -\boldsymbol{M}'^{-1}(p\boldsymbol{M}' + \boldsymbol{R}')\boldsymbol{I}' + \boldsymbol{M}'^{-1}\boldsymbol{U}' \tag{13}$$

where $\boldsymbol{M}' = \boldsymbol{BMB}^{\mathrm{T}}$, $\boldsymbol{R}' = \boldsymbol{BRB}^{\mathrm{T}}$.

Equation (13) is the standard state equation with the independent loop current $\boldsymbol{I}'$ as the variable, and is also the mathematical model of the MPABE with the rectifier. When the parameters and initial conditions of the system are known, the loop current at any time can be calculated. Then, the branch voltage $\boldsymbol{U}$ and branch current $\boldsymbol{I}$ can be obtained by substituting $\boldsymbol{I}'$ into (10) and (12).

III. Simulation and Experimental Analysis of AWSC

A. Introduction of Experimental Device

In order to verify the correctness of the simulation model, an 11-phase prototype is designed and manufactured according to the structure of the actual exciter. In order to facilitate the measurement of the electrical quantities of armature winding and diode in the experiment, the prototype is designed as a rotating-excitation structure. The basic parameters of the prototype are shown in Table I

Some taps are installed on different positions of the armature windings, as shown in Fig. 4. These taps are used to connect the diodes, measure the electrical quantities of armature windings, and perform short-circuit experiments.

The actual experimental device is shown in Fig. 5. In the experiment, a dc motor driven by Siemens 6RA80 regulater is used to drive the prototype, which maintains the same speed

TABLE I
Basic Parameters of 11-Phase Exciter Prototype

Parameter	Value	Parameter	Value
Apparent power	22.3 kVA	Phase voltage	120 V
Field voltage	60.33 V	Field current	12.97 A
Pitch	8	Rotary speed	1000 r/min
Slot number	77	Pole-pair number	5

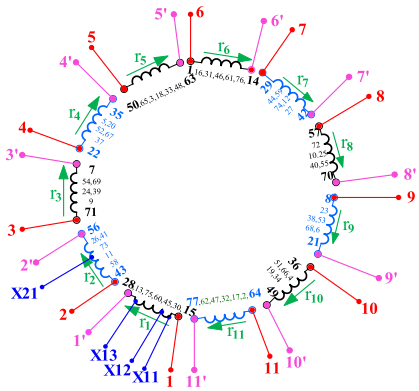

Fig. 4. Taps on the armature windings.

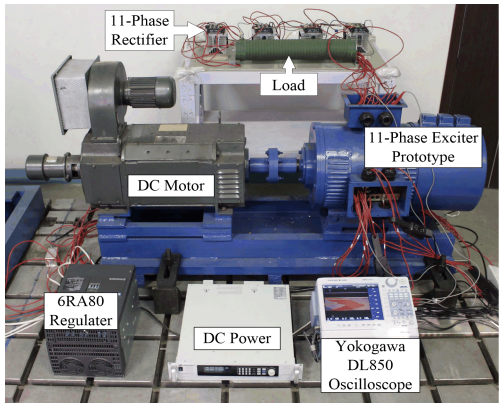

Fig. 5. Actual experimental device.

before and after the fault through the closed-loop speed control. The field winding of the prototype is supplied by a dc power, and the armature windings are connected with the series resistance and inductance load ($R_{\mathrm{dc}} = 10.6\ \Omega$, $L_{\mathrm{dc}} = 0.357$ H) by the 11-phase rectifier.

B. Prototype Experimental Verification of Mathematical Model

In order to ensure the safety of the experiment and avoid the damage of the prototype due to the overcurrent caused by the AWSC fault, the experiments are carried out under low field current. The field current before the fault is set as 2.46 A. In addition, the rotor speed is kept at 960 r/min and the fundamental frequency of induced armature EMF is 80 Hz. The experiment waveforms are recorded by Yokogawa DL850 recorder, while the sampling frequency is 20 kS/s.

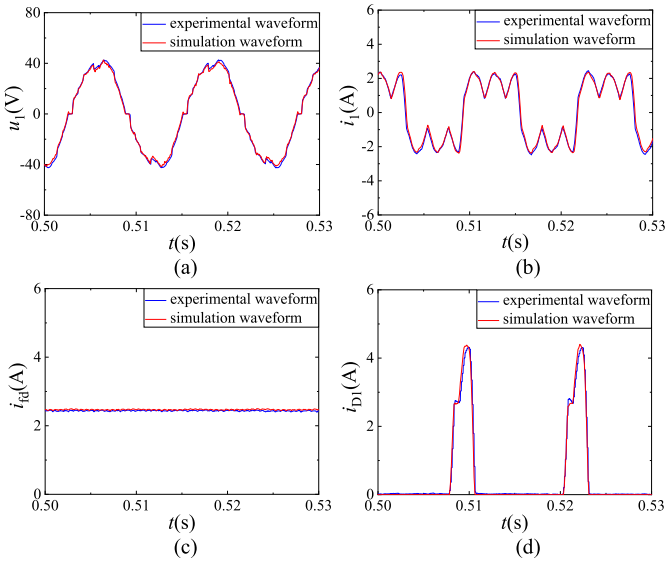

Fig. 6. Experimental and simulation waveforms in the normal operation. (a) Armature voltage of Phase 1. (b) Armature current of Phase 1. (c) Field current. (d) Diode current of upper arm of Phase 1.

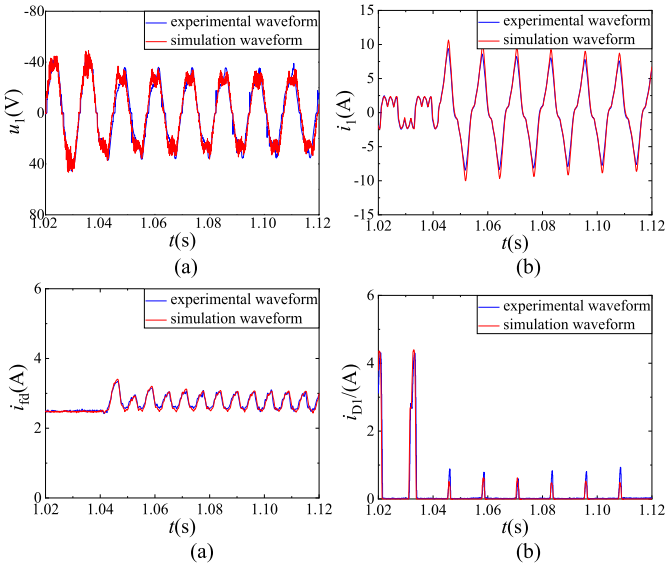

Fig. 7. Experimental and simulation waveforms under the AWSC fault between tap "1" and tap "X12". (a) Armature voltage of Phase 1. (b) Armature current of Phase 1. (c) Field current. (d) Diode current of upper arm of Phase 1.

Fig. 6 and are the experimental and simulation waveforms of 11-phase prototype under normal operation and AWSC fault between tap "1" and tap "X12" (see the f1 in Fig. 2). The fault time in experiments is the same as that in the simulation, which is about $t = 1.04$ s. It can be seen from Fig. 6 and that the experiment and simulation waveforms agree well with each other no matter in the normal operation or under the AWSC fault, which verifies the correctness of the rapid simulation model. At the same time, the rapid simulation model can complete the calculation of a complete process from fault occurrence to postfault steady state in only about three minutes, which

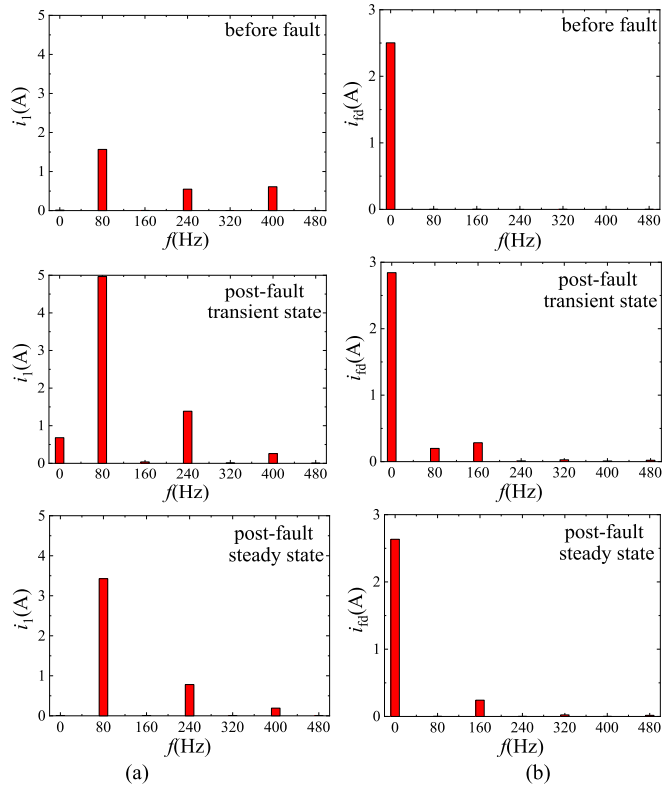

Fig. 8. Current spectrum diagram under AWSC fault [(a) armature current (b) excitation current].

indicates that the rapid calculation model proposed in this article has great advantages over FEM simulation in calculation speed while ensuring sufficient simulation accuracy.

C. Fault Characteristics

In order to further analyze the fault harmonic characteristics, we perform Fourier analyses for one period in the normal operation ($t = (0.5$ s–0.5625 s)), the first period after the fault ($t = 1.042$ s–1.1045 s) and one period in the postfault steady state ($t = 1.2$ s–1.2625 s) of the armature current waveform and field current waveform, respectively. The fundamental frequency is 80 Hz, and the frequency spectrum of each current is obtained, as shown in Fig. 8. From further observation, we can find that as follows.

1) *Armature current:* In normal operation, the armature current mainly contains odd-order harmonic currents; during the post-fault transient process, the dc component and fundamental current in the armature current increase significantly, and the third harmonic current increases slightly. In the postfault steady state, the dc component and third harmonic current attenuate to their level in normal operation, and the fundamental current decreases slightly and reaches stability, but it is still far greater than that in normal operation.
2) *Excitation current:* In normal operation, the excitation current does not contain harmonic current expect dc component; during postfault transient process, in addition to

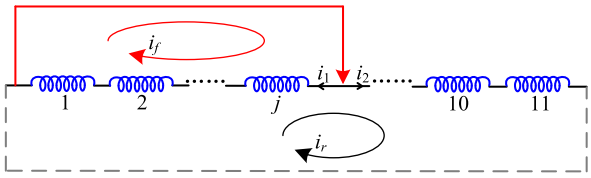

Fig. 9. Current circuit of armature winding after AWSC fault.

dc component, the fundamental current, and the second harmonic current also increase significantly; In the post-fault steady state, the dc component will decay to the same as that in normal operation. At this time, the excitation current mainly contains the second harmonics, but no longer contains the large fundamental component in the postfault transient process.

In addition, this article also simulates the AWSC fault between different taps of the 11-phase prototype (including interturn short-circuit fault in phase and phase-to-phase short-circuit fault). The fault harmonic characteristics is the same as that the fault between tap "1" and tap "X12". In order to save space, it will not be repeated.

IV. Mechanism of the Fault Characteristics

A. Fault Characteristics of Armature Current

The armature winding of 11-phase brushless exciter adopts an annular structure with end-to-end connection, and the armature winding connection table is shown in Appendix A. It can be known that the adjacent armature windings differ by $4\pi/11$ electrical angle in space, consequently, the potential in the two adjacent armature windings also differ by $4\pi/11$ electrical angle in time.

The analysis method of AWSC faults at different positions of 11-phase brushless exciter is similar. Taking the integer phase short-circuit fault as an example, Fig. 9 shows the current circuit under the j-phase ($j < 11$) AWSC fault. As can be seen, the armature winding is divided into two branches to supply power to the fault point in parallel. At this time, two fault currents will be added to the winding, as shown in Fig. 9, which are fault short-circuit current i_f and armature winding circulating current i_{r}, respectively. However, since the spatial position of the 11-phase armature winding is symmetrical, and the amplitude and phase of i_{r} flowing through each phase armature winding are equal, each phase winding will produce a symmetrical magnetomotive force (MMF) with the same time angle and a sequential spatial difference of $4\pi/11$ electrical angle. Therefore, the MMF generated by i_{r} will be zero after the spatial synthesis of the 11-phase armature winding. Therefore, as described in (1), only one fault current branch is added actually after fault. Therefore, there is only one fault current branch to consider here, which is i_f.

We assume the internal potential of the phase k armature winding as

$$u_k = U \sin\left[\omega t - (k-1)\frac{4\pi}{11}\right] \tag{14}$$

where U is the amplitude of the potential in the phase k armature winding and ω is the synchronous rotary speed.

The potential between two short-circuit points is the sum of the potential in series of the fault winding. From (14), it can be calculated that the potential in the fault winding is

$$\begin{aligned} u_{1,2,\ldots,j} &= U\sin\omega t + U\sin\left(\omega t - \frac{4\pi}{11}\right) \\ &\quad + \cdots + U\sin\left[\omega t - (j-1)\frac{4\pi}{11}\right] \\ &= U\frac{\sin(2j\pi/11)}{\sin(2\pi/11)}\sin\left[\omega t - (j-1)\frac{2\pi}{11}\right]. \end{aligned} \tag{15}$$

Assuming that the internal reactance of each phase armature winding of the exciter is equal to Z. When the mutual inductance between windings is ignored, the short-circuit current i_f can be deduced as

$$i_f = \frac{u_{1,2,3\ldots j}}{jZ//(11-j)Z} = \frac{11}{j(11-j)Z}u_{1,2\ldots j}. \tag{16}$$

In fact, when the AWSC fault occurs, the current in faulty armature winding can increase to tens of times as much as that in normal operation (similar to the short-circuit fault of generator stator winding). However, the inductance in the armature winding prevents the current from changing suddenly. Therefore, at the fault moment, an additional aperiodic component (dc component) will be generated in the faulty armature current to keep the flux linkage of short-circuit loop from a sudden change. That is, in the initial stage of fault occurrence, the short-circuit current i_f will contains both periodic component i_{p} and aperiodic component i_{ap}. It can be deduced that the short-circuit current i_f in the postfault transient process is

$$\begin{aligned} i_f &= i_{\mathrm{p}} + i_{\mathrm{ap}} \\ &= \frac{11U_1}{j(11-j)Z}\frac{\sin(2j\pi/11)}{\sin(2\pi/11)}\sin\left[\omega t - (j-1)\frac{2\pi}{11}\right] + i_{\mathrm{ap}}. \end{aligned} \tag{17}$$

It can be seen from (17) that in the postfault transient process, the fault components in the armature winding are mainly fundamental current and transient aperiodic component. In fact, in the process of the postfault transient state, there will also be transient aperiodic components (dc component) in the excitation winding. As in normal operation, the increased dc components in excitation winding will also induce additional odd-order harmonic currents in the armature winding. When the fault reaches the steady state, the aperiodic component in the stator and rotor attenuates to zero, and the additional odd-order harmonic currents induced by them in the armature windings also attenuates to zero. At this time, only the fundamental current is contained in armature winding.

B. Fault Characteristics of Excitation Current

When the fault current i_f flows through the phase k armature winding, the spatial distribution of the MMF generated in space is still a rectangular wave. Since the armature windings of MPABE are designed as fractional-slot and wave structure, the

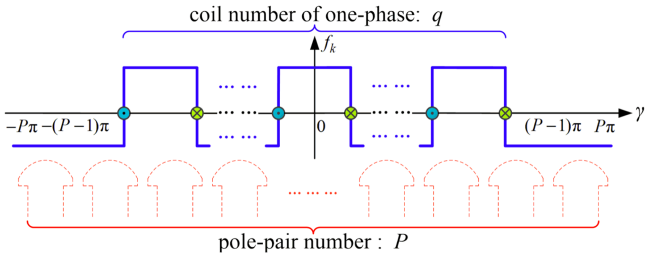

Fig. 10. Space MMF generated by one-phase armature winding.

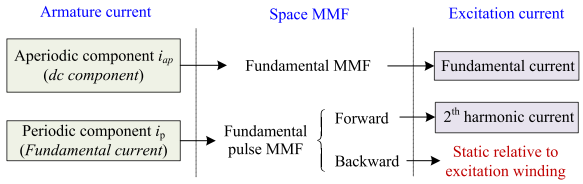

Fig. 11. Induction process between stator and rotor currents.

space MMF generated by one-phase armature winding under each pair of magnetic poles is different, which distribution period is $2P\pi$. Assuming that one-phase winding consists of q coils (the value of $q/2P$ is fractional, where P is the pole-pair number), the distribution of the space MMF generated by one-phase armature winding in rotor coordinates is shown in Fig. 10.

The Fourier decomposition of one-phase armature winding MMF with period $2P\pi$ shows that it contains n/P ($n = 12,3\ldots$) harmonic MMFs, which will establish the corresponding magnetic field in the air gap. However, since the field winding is wound in opposite directions under south-poles and north-poles, the total EMF induced by the fractional, and even-order magnetic field is zero. Therefore, only the fundamental and odd-order harmonic MMF need to be considered.

It can be assumed that space-time expression of the νth ($\nu = 13,5\ldots$) harmonic MMF generated by i_f in the phase k armature winding as

$$f_{k,i_f} = F_{i_f} i_f \sin \upsilon \left[\gamma - (k-1)\frac{4\pi}{11}\right] \tag{18}$$

where F_{i_f} is the amplitude of the armature harmonic MMF and γ is the electrical radian on the rotor circumferential.

$\alpha$is the electrical radian on the stator circumference, the relationship between α and γ is as follows:

$$\gamma = \alpha + \omega t. \tag{19}$$

The fault armature current includes periodic and aperiodic component, both of which will produce corresponding MMF in the air gap of the exciter. Then, the MMF of the short-circuited j-phase armature winding can be derived from (17), (18), and (19), which can be written as

$$\begin{aligned} f_{i_f} &= F_{i_f} i_f \sum_{k=1}^{j} \sin \upsilon \left[\alpha + \omega t - (k-1)\frac{4\pi}{11}\right] \\ &= F_{i_p} I_p \sin\left[\omega t - (j-1)\frac{2\pi}{11}\right] \\ &\quad \times \sin \upsilon \left[\alpha + \omega t - (j-1)\frac{2\pi}{11}\right] \\ &\quad + F_{i_{ap}} I_{ap} \sin \upsilon \left[\alpha + \omega t - (j-1)\frac{2\pi}{11}\right] \\ &= f_p + f_{ap} \end{aligned} \tag{20}$$

where i_p and i_{ap} are the amplitudes of periodic and aperiodic component currents, and the corresponding MMF amplitudes are F_{i_p} and $F_{i_{ap}}$, respectively.

It can be seen from (20) that the MMF f_p generated by the periodic component is the pulsating MMF on the stator spatial coordinate, which can be decomposed into spatial forward and backward MMFs, then (20) can be written as

$$\begin{aligned} f_p &= \frac{1}{2} F_{i_p} I_p \cos\left[\upsilon\alpha + (\upsilon-1)\omega t - (\upsilon-1)(j-1)\frac{2\pi}{11}\right] \\ &\quad + \frac{1}{2} F_{i_p} I_p \cos\left[\upsilon\alpha + (\upsilon+1)\omega t - (\upsilon+1)(j-1)\frac{2\pi}{11}\right] \\ f_{ap} &= F_{i_{ap}} I_{ap} \sin \upsilon \left[\alpha + \omega t - (j-1)\frac{2\pi}{11}\right]. \end{aligned} \tag{21}$$

As can be seen from (21), In the MMF f_p generated by the periodic component, the speed of the νth forward harmonic MMF relative to the stator is $(\nu+1)/\nu$. Hence, it will induce $(\nu+1)$th EMF in the stator field winding. Similarly, the speed of the νth backward harmonic MMF relative to the stator is $(\nu\text{-}1)/\nu$ and will induced $(\nu\text{-}1)$th EMF in the stator field winding. Since the value of ν is odd ($\nu = 13,5\ldots$), the magnetic field established by the periodic component will induce even-order harmonic EMF in the excitation winding. For the MMF f_{ap} generated by the aperiodic component, the νth harmonic MMF will generate a spatial magnetic field rotating relative to the stator winding at synchronous speed in the air gap, which will induce νth harmonic EMF in the field winding.

Considering that the exciter current mainly generates the fundamental MMF in the space air gap, the aperiodic component will establish the fundamental magnetic field stationary relative to the rotor but rotating at the synchronous speed relative to the stator in space, so the fundamental current is induced in the stator excitation winding, as shown in Fig. 11. The periodic component only contains the fundamental current, which will establish a pulsative MMF in the air gap. The forward component of the pulsative MMF rotates at twice the synchronous speed relative to the stator, which mainly induces the second harmonic current in the excitation winding, while the backward component is stationary relative to the stator and does not induce current in the stator excitation winding.

To sum up, in the postfault transient process of AWSC, the armature fault current will mainly produce the fundamental and second harmonic current in the excitation winding. In the postfault steady state of fault, the fundamental current in the excitation current will decay to zero. At this time, the excitation current mainly contains the second harmonic current.

C. Variation Law of Fault Characteristic Quantity

Since the fault with the smallest characteristic quantity may not be the 1-coil AWSC, it is possible that the more the number of short-circuited coils, the smaller the fault characteristic quantity, which will lead to insufficient protection sensitivity and misjudgment. Therefore, in order to reliably diagnose the AWSC fault with any number of coils, it is necessary to theoretically analyze the variation law of the fault characteristic quantity with the number of short-circuited coils, so as to find the smallest characteristic quantity and then verify the sensitivity of protection.

Different from the general star structure motor, all windings of the annular brushless exciter are connected in series into a ring and evenly distributed on the rotor. Therefore, the AWSC fault in phase, phase to phase, or integer phase at different positions can be analyzed by the number of the actually shorted coils. The armature winding of each phase of 11-phase exciter is composed of 7 coils, so the short-circuit fault of two-phase armature winding is 14-coil short-circuit fault. The adjacent two-phase armature windings differ by $4\pi/11$ electrical angle in space, so the potential in the two adjacent coils at any position differs by 4 $\pi/77$ electrical angle in time.

As the fault changes from transient to steady state, the aperiodic current in armature winding will decay to zero. Therefore, only the law of the characteristic quantity in postfault steady-state (i.e., the second harmonic current) is analyzed. Assuming that the number of short-circuited coils in the armature winding is x, the MMF of the short-circuited coil can be synthesized in space, which can be written as

$$\begin{aligned} f_{\mathrm{p}} &= F_{i_f} i_f \sum_{k=1}^{x} \sin\left[(\gamma-(k-1)\frac{4\pi}{77}\right] \\ &= F_x \sin\left[\omega t-(k-1)\frac{2\pi}{77}\right]\sin\left[\gamma-(k-1)\frac{2\pi}{77}\right] \end{aligned} \quad (22)$$

where F_x is the amplitude of synthetic MMF generated by x short-circuited coils in space.

The expression of F_x can be further calculated according to machinery principles and (20) as follows:

$$\begin{aligned} F_x &= \frac{77U_1}{x(77-x)Z'}\frac{\sin^2(2x\pi/77)}{\sin^2(2\pi/77)}\frac{2Nk_{dp}}{\pi P} \\ &= \frac{77U_1}{x(77-x)Z'}\frac{\sin^2(2x\pi/77)}{\sin^2(2\pi/77)}\frac{2N}{\pi P}\frac{\sin(q(\theta/2))}{q\sin(\theta/2)}\sin\frac{y\pi}{2} \end{aligned} \quad (23)$$

where Z' is the impedance of one armature winding coil, U_1 is the amplitude of potential in one armature winding coil, n is the number of parallel branches of phase winding, q is the number of slots per pole per phase, θ is the slot pitch angle, and y is the winding short pitch ratio.

It can be found from (23) that the amplitude F_x is directly determined by the number of shorted coils, i.e., x. The variation law of fault MMF amplitude under different number of short-circuited coils is shown as Fig. 12. It can be found from Fig. 12 that when the number of short-circuited coils increases from 1–16, the amplitude of the corresponding fault MMF also increases. When the number of short-circuited coils is 16, the amplitude of the fault MMF reaches the maximum, and then decreases until the fault MMF reaches the minimum when 38 coils are short-circuited. The relative size distribution of fault MMF amplitude corresponding to short-circuit fault of integer phase armature winding is shown in Fig. 12. Since the armature winding is of annular structure, the distribution of MMF under 1–38 coils short-circuited is the same as that of 39–78 coils short-circuited.

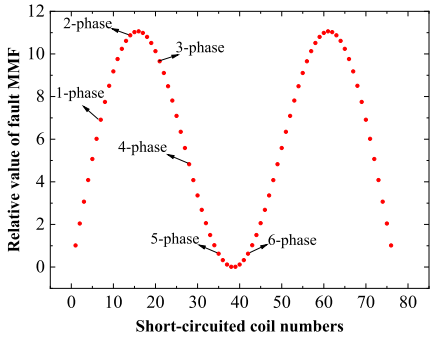

Fig. 12. Variation of MMF with the number of short-circuited coils.

The fault MMF will establish the harmonic magnetic field with different pole pairs and rotating speed in air gap, which will induce the fault characteristic harmonic EMF on the excitation winding. The amplitude of the induced harmonic EMF is directly proportional to the amplitude of the spatial MMF. Therefore, it can be seen from Fig. 12 that for the 11-phase annular brushless exciter, the smallest characteristic quantity is not the 1-coil short-circuit fault, but the 38-coil (the same as 39-coil) AWSC fault. Moreover, when 16-coil armature winding is short-circuited, the characteristic quantity is the largest.

In order to verify the theoretical analysis of the fault characteristics and the variation law of characteristic quantity, the verified rapid simulation mathematical model is used to simulate the metal short-circuit faults with different coil numbers. The average simulation time is about 15 min. The simulated fault excitation current is shown in Fig. 13. It can be found that the ripple of excitation current waveform under 2-phase AWSC fault is the most obvious, and the waveform of excitation current under 5-phase AWSC is consistent with that under six phase AWSC. At the same time, compared with 1-coil fault, the excitation current ripple is significantly smaller under 38-coil AWSC fault. In the actual operation, since the short-circuit current in armature windings will be shunted by the diode and the load, especially when more coil armature windings are short-circuited, the absolute magnitude of the simulated excitation current will not be exactly consistent with the theoretical analysis. However, the variation law of fault excitation current waveform with the number of short-circuited coils in the simulation is completely consistent with Fig. 12, which verifies the theoretical analysis.

V. Design of Fault Diagnosis Method

A. Principle of Diagnosis Method

The theoretical analysis and simulation results are consistent, which show that when the armature winding of the exciter has a

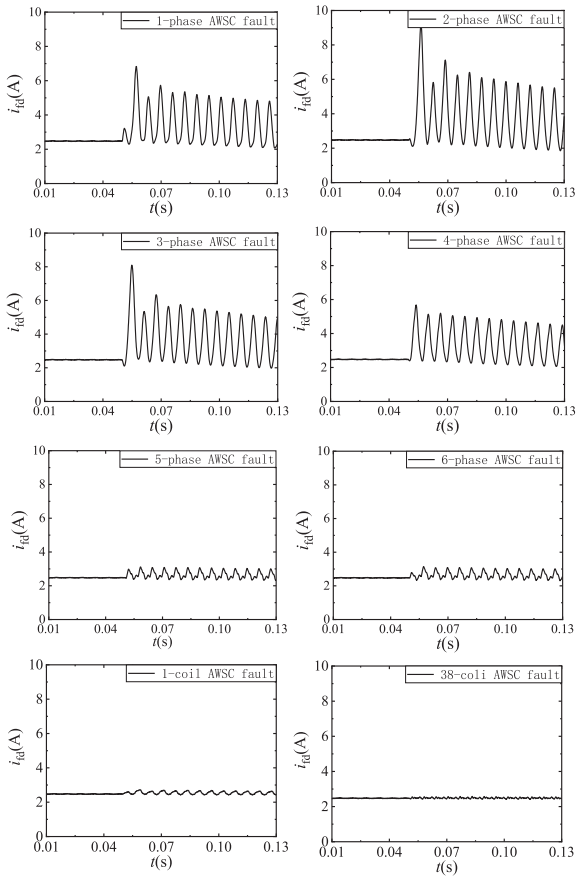

Fig. 13. Waveform of excitation current under short circuit fault of armature winding with different number of coils.

TABLE II
HARMONICS OF THE FIELD CURRENTS OF THE 11-PHASE PROTOTYPE.

Harmonics	dc(A)	1st	2nd	$I_{1,2}\%$
Normal operation	2.503	0.003	0.002	0.002
Post fault transient state	2.843	0.199	0.284	0.122
Post fault steady state	2.634	0.002	0.242	0.092

short-circuit fault, the fundamental current and the second harmonic current will mainly appear in the excitation current. These fault currents can be used to diagnose the AWSC fault in theory. However, in practice, when the exciter works at different excitation current levels, the characteristic quantities in the excitation current are also different under the same AWSC fault. Therefore, it is necessary to "standardize" the fault characteristic quantities with the dc component of excitation current as the reference, i.e., the ratio of the total effective value of the fundamental current and the second harmonic current to the dc component can be taken as the fault diagnosis criterion, which is defined as

$$I_{1,2}\% = \frac{\sqrt{I_1^2 + I_2^2}}{I_{\rm dc}} \tag{24}$$

where I_1 and I_2 are the effective value of the fundamental and the second harmonic of stator field current, respectively, and $I_{\rm dc}$ is the effective value of dc component of stator field current.

TABLE III
SENSITIVITY COEFFICIENT UNDER SHORT-CIRCUIT FAULT WITH DIFFERENT COIL NUMBER

Harmonics	$I_{1,2}\%$	$K_{\rm sen}$
1-coil AWSC	0.030	1.5
1-phase AWSC	0.297	14.9
2-phase AWSC	0.355	17.8
3-phase AWSC	0.315	15.8
4-phase AWSC	0.267	13.3
5-phase AWSC	0.071	3.5
6-phase AWSC	0.071	3.5
38-coil AWSC	0.007	0.3

Table II shows the harmonic results of excitation current when the short-circuit fault between tap "1" and tap "X12" occurs in the prototype. The postfault transient state in the table is the first period after fault. It can be found that during normal operation of the exciter, the value of $I_{1,2\%}$ in the excitation current is 0.003. After the fault occurs, the value of $I_{1,2\%}$ in the postfault transient state and postfault steady state will increase by more than 30 times.

The preset threshold value of the criterion can be defined as $I_{1,2,\rm set\%}$, which should be larger than that in the normal operation. According to the results in Table II, $I_{1,2,\rm set\%}$ can be taken as 0.02 (10 times of that in normal operation); When the value of $I_{1,2}\%$ exceeds $I_{1,2,\rm set}\%$, it can be judged that there is an AWSC fault in the MPABE.

B. Sensitivity Analysis of Diagnostic Methods

The diagnose sensitivity coefficient $K_{\rm sen}$ is defined as the ratio of $I_{1,2\%}$ and $I_{1,2,\rm set\%}$ in the case of fault, which can be written as

$$K_{\rm sen} = \frac{I_{1,2}\%}{I_{1,2,\rm set}\%}. \tag{25}$$

When the sensitivity coefficient $K_{\rm sen}$ is larger than 1.3, it is considered that the method can reliably diagnose the AWSC fault of this number of coils, otherwise it is the opposite.

Obviously, when the number of coils with AWSC fault is different, the effective value of $I_{1,2\%}$ in the excitation current is also different. Accordingly, the sensitivity coefficient of diagnostic method monitoring is also different. Therefore, the postfault steady state excitation current after the short-circuit fault of different coil numbers is analyzed by Fourier. The harmonic results and sensitivity coefficient are shown in Table III. It can be found that the sensitivity coefficient under 1-coil short-circuit fault is 1.5, which is larger than 1.3. Consequently, the method can reliably diagnosis the fault. From the content of second harmonic under different faults, it can be seen that the variation law of characteristic quantity under short-circuit of integer phase armature winding is consistent with the theoretical analysis. At the same time, the smallest fault characteristic quantity is not 1-coil AWSC fault, but the 38-coil AWSC fault. Moreover, in the case of 38-coil short-circuit fault, the diagnose sensitivity coefficient is far less than 1. Therefore, the diagnosis method

TABLE IV
k VALUE UNDER ARMATURE WINDING SHORT CIRCUIT FAULT

Harmonics	dc(A)	1st(A)	2nd(A)	k
Normal	2.475	0.003	0.001	0.3
1-coil AWSC	2.535	0.002	0.076	38.0
One-phase AWSC	2.527	0.001	0.751	751.0
Two-phase AWSC	2.482	0.001	0.882	882.0
Three-phase AWSC	2.494	0.001	0.786	786.0
Four-phase AWSC	2.500	0.002	0.667	333.5
Five-phase AWSC	2.632	0.002	0.186	93.0
Six-phase AWSC	2.633	0.002	0.186	93.0
38-coil AWSC	2.484	0.002	0.023	11.5

cannot identify the short-circuit fault of this number of coils, which means the diagnostic method has a dead zone when 38-coil armature winding are short-circuited.

For the general annular brushless exciter with other phase numbers, the fault characteristic quantity in the excitation current during AWSC fault is not linearly related to the number of short-circuited coils, but the fault MMF is minimized when exactly half of the armature winding coils are short-circuited. Moreover, with the difference of electric potential between two adjacent armature windings, the minimum value may be much smaller than the threshold value, resulting in a larger dead zone for short-circuit fault protection.

C. Optimization of the Diagnostic Method

For the 11-phase annular brushless exciter, when the armature winding is short-circuited by 38 coils, the fault characteristic quantity in the excitation current is the smallest, which is smaller than the preset threshold value of the protection criterion, resulting in the failure of diagnose. However, in fact, the fundamental current in the excitation current will gradually decay to zero during the postfault transient process, while the second harmonic current is basically stable. Therefore, the ratio of I_2 to I_1 will continue to increase, while it is very small during normal operation. Hence, in theory, the ratio of I_2 to I_1 can be used to identify slight AWSC fault. Meanwhile, in order to avoid misjudgment of the protection when the excitation current only contains I_1 but exceeds the threshold value of criterion I ($I_{1,2,\mathrm{set}}\%$), criterion II is added as follows:

$$k = I_2/I_1. \tag{26}$$

Table IV shows the value of k during normal operation of exciter and postfault steady state of AWSC fault. It can be found that the excitation current basically does not contain harmonic current during normal operation. In addition, since I_1 is slightly greater than I_2, the value of k is very small, about 0.3. In the postfault steady state of AWSC fault, the k value will increase significantly. It can be found that even for the 38-coil short-circuit fault, the k value of excitation current in the postfault steady state will increase significantly to about 40 times that in normal operation. Therefore, the criterion II can be used to identify the AWSC of this number of coils.

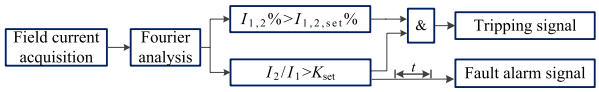

Fig. 14. Diagnosis method of AWSC fault.

D. Complete Fault Diagnosis Process

The optimized diagnosis method is shown in Fig. 14. When criterion I and criterion II are met at the same time, the protection sends the trip signal. For the short-circuit fault that does not meet criterion I but meet criterion II, since the short-circuit fault of this number of coils has a very slight impact on the exciter, the protection is designed to output only the alarm signal. Moreover, the protection will always monitor the development of the fault after discovering the slight short-circuit fault in the initial stage to determine whether tripping is required. Considering the possible interference of excitation current, the actual protection device is also set with a certain time delay. In fact, the high threshold setting value of the criterion II allows the protection make a decision when the postfault transient process is almost over, which delays the protection and eliminates short-term interference.

E. Threshold Setting

As can be seen from Fig. 14, there are two threshold values that need to be determined for protection: $I_{1,2,\mathrm{set}}\%$ and K_{set}. However, it should be noted that the determination of the value of $I_{1,2,\mathrm{set}}\%$ and K_{set} does not require any AWSC faults; instead, it requires only the excitation current data during normal operation. Then, the values of $I_{1,2,\mathrm{normal}}\%$ and k_{normal} in the excitation current under normal operation need to be measured. The determination of the threshold value is as follows.

1) $I_{1,2,set}\%$*:* Its setting value needs to be greater than the value of $I_{1,2}\%$ in normal operation to effectively avoid the possible interference and deviation. Then, the $I_{1,2,\mathrm{set}}\%$ value can be defined as

$$I_{1,2,set}\% = k_{rel,1} I_{1,2,\mathrm{normal}}\% \tag{27}$$

where $k_{rel,1}$ is the reliability coefficient. Since the harmonics in the excitation current under fault will increase significantly compared with that of normal operation, $k_{rel,1}$ can be taken from 5–10 according to the requirements of reliability.

2) K_{set}*:* The value of K_{set} only needs to be greater than the value of k in normal operation. Then, the K_{set} value can be defined as

$$K_{\mathrm{set}} = k_{rel,2} k_{\mathrm{normal}}. \tag{28}$$

Since I_1 is slightly greater than I_2 in normal operation, the value of k is less than 1, but it will increase significantly after the AWSC fault. Therefore, the reliability coefficient $k_{rel,2}$ can be taken from 5–10 according to the requirements of reliability.

F. Prototype Experimental Verification of the Diagnosis Method

In order to verify the reliability of the diagnosis method, we compiled the corresponding protection program according to

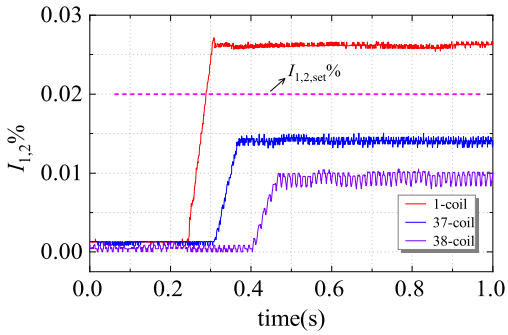

Fig. 15. Variation of $I_{1,2\%}$ effective value in excitation current.

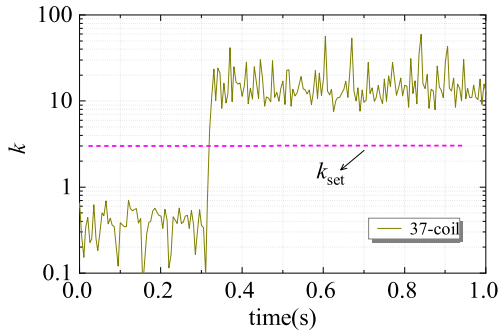

Fig. 16. k value under 37-coil short-circuit fault.

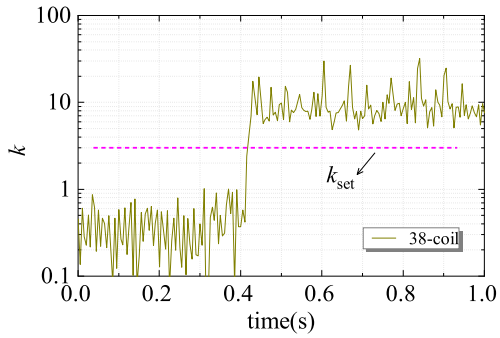

Fig. 17. k value under 38-coil short-circuit fault.

the trigger logic of the abovementioned protection, and further carried out the 1-coil, 37-coil, and 38-coil AWSC fault experiments on the prototype. According to the experimental results of the prototype and the method of determining the threshold value, the preset threshold value of $I_{1,2,\mathrm{set}}\%$ and K_{set} can be taken as $0.02(k_{rel,1} = 10)$ and $3(k_{rel,2} = 10)$, respectively.

During the experiment, the stator excitation current of the exciter is collected in real time through the hall coil with high sensitivity, and the analysis results are shown in Fig. 15–17. It can be found from Fig. 15 that when 1-coil short-circuit fault occurs in the armature winding, the $I_{1,2\%}$ effective value of the excitation current will reliably exceed the threshold setting value $I_{1,2\mathrm{set}\%}$. For the 37-coil and 38-coil short-circuit faults in which the $I_{1,2\%}$ effective value is smaller than the threshold setting value $I_{1,2\mathrm{set}\%}$, it can be found from Figs. 16 and 17 that their k value will reliably exceed the threshold setting value k_{set} of criterion II, Therefore, the protection judges that there is a slight short-circuit fault in the armature winding at this time and sends an alarm signal.

VI. Conclusion

In this article, a rapid simulation mathematical model of MPABE with AWSC fault is presented. Furthermore, the simulation, experiment and theoretical research on the AWSC fault in MPABE are carried out, respectively. The fault harmonic characteristics of the stator currents are obtained: in the postfault transient process, the stator excitation current is mainly fundamental, and the second harmonic current, while in the postfault steady state, it only contains the second harmonic current.

Based on the fault characteristics, this article proposes a diagnosis method for AWSC fault of MPABE. The experimental results have demonstrated that the diagnosis method proposed in this article is sensitive and reliable, and can realize 100% protection of armature winding. In addition, this article finds that some AWSC faults have little impact on the exciter, so the exciter can continue to work. Therefore, the fault redundant operation and control of MPABE may be an interesting topic in the future.

Appendix

The winding connection table of 11-Phase Exciter Prototype.

Phase 1: 1-16-31-46-61-76-14. Phase 2: 29-44-59-74-12-27-42.
Phase 3: 57-72-10-25-40-55-70. Phase 4: 8-23-38-53-68-6-21.
Phase 5: 36-51-66-4-19-34-49. Phase 6: 64-2-17-32-47-62-77.
Phase 7: 15-30-45-60-75-13-28. Phase 8: 43-58-73-11-59-41-56.
Phase 9: 71-9-24-39-54-69-7. Phase 10: 22-37-52-67-5-20-35.
Phase 11: 50-65-3-18-33-48-63

References

[1] Z. Gu, "History review of nuclear reactor safety," *Ann. Nucl. Energy*, vol. 120, pp. 682–690, 2018, doi: 10.1016/j.anucene.2018.06.023.
[2] T. Zouaghi and M. Poloujadoff, "Modeling of polyphase brushless exciter behavior for failing diode operation," *IEEE Trans. Energy Convers.*, vol. 13, no. 3, pp. 214–220, Sep. 1998.
[3] H. Gorginpour, "Optimal design of brushless AC exciter for large synchronous generators considering grid codes requirements," *IET Gener., Transmiss. Distrib.*, vol. 12, no. 17, pp. 3954–3962, Sep. 2018.
[4] X. Jia, Q. Li, J.-S. Lai, and B.-M. Song, "Analysis of polyphase brushless exciter," *IEEE Trans. Ind. Appl.*, vol. 37, no. 6, pp. 1720–1726, Nov./Dec. 2001.
[5] X. H. Wang, Y. G. Sun, B. Ouyang, W. J. Wang, Z. Q. Zhu, and D. Howe, "Transient behavior of salient-pole synchronous machines with internal stator winding faults," *IEEE Proc.-Electric Power Appl.*, vol. 149, no. 2, pp. 143–151, Mar. 2002.
[6] X. Tu, L.-A. Dessaint, M. El Kahel, and A. Barry, "Modeling and experimental validation of internal faults in salient pole synchronous machines including space harmonics," *Math. Comput. Simul.*, vol. 71, pp. 425–439, 2006.
[7] M. Ojaghi and V. Bahari, "Rotor damping effects in dynamic modeling of three-phase synchronous machines under the stator interturn faults-winding function approach," *IEEE Trans. Ind. Appl.*, vol. 53, no. 3, pp. 3020–3028, May/Jun. 2017.
[8] Y. He, Y. Zhang, M. Xu, X. Wang, and J. Xiong, "A new hybrid model for electromechanical characteristic analysis under SISC in synchronous generators," *IEEE Trans. Ind. Electron.*, vol. 67, no. 3, pp. 2348–2359, Mar. 2020, doi: 10.1109/TIE.2019.2907450.
[9] D. G. Dorrell and K. Makhoba, "Detection of inter-turn stator faults in induction motors using short-term averaging of forward and backward rotating stator current phasors for rapid prognostics," *IEEE Trans. Mag.*, vol. 53, no. 11, Nov. 2017, Art. no. 1700107.

[10] M. Ojaghi, M. Sabouri, and J. Faiz, "Performance analysis of squirrel-cage induction motors under broken rotor bar and stator inter-turn fault conditions using analytical modeling," *IEEE Trans. Mag.*, vol. 54, no. 11, Nov. 2018, Art. no. 8203705.
[11] G. Mirzaeva and K. I. Saad, "Advanced diagnosis of stator turn-to-turn faults and static eccentricity in induction motors based on internal flux measurement," *IEEE Trans. Ind. Appl.*, vol. 54, no. 4, pp. 3961–3970, Jul./Aug. 2018.
[12] M. Afshar, A. Tabesh, M. Ebrahimi, and S. A. Khajehoddin, "Stator short-circuit fault detection and location methods for brushless DFIMs using nested-loop rotor slot harmonics," *IEEE Trans. Power Electron*, vol. 35, no. 8, pp. 8559–8568, Aug. 2020.
[13] L. L. Wang et al., "Fault diagnosis based on current signature analysis for stator winding of doubly fed induction generator in wind turbine," in *Proc. Int. Symp. Elect. Insulating Mater.*, 2014, pp. 233–236.
[14] R. Hu, J. Wang, A. R. Mills, E. Chong, and Z. Sun, "High-Frequency voltage injection based stator interturn fault detection in permanent magnet machines," *IEEE Trans. Power Electron*, vol. 36, no. 1, pp. 785–794, Jan. 2021, doi: 10.1109/TPEL.2020.3005757.
[15] J. Urresty, J. Riba, and L. Romeral, "Diagnosis of interturn faults in PMSMs operating under nonstationary conditions by applying order tracking filtering," *IEEE Trans. Power Electron.*, vol. 28, no. 1, pp. 507–515, Jan. 2013, doi: 10.1109/TPEL.2012.2198077.
[16] J. Hang, J. Zhang, M. Cheng, and J. Huang, "Online interturn fault diagnosis of permanent magnet synchronous machine using zero-sequence components," *IEEE Trans. Power Electron.*, vol. 30, no. 12, pp. 6731–6741, Dec. 2015, doi: 10.1109/TPEL.2015.2388493.
[17] B. M. Ebrahimi and J. Faiz, "Feature extraction for short-circuit fault detection in permanent-magnet synchronous motors using stator-current monitoring," *IEEE Trans. Power Electron.*, vol. 25, no. 10, pp. 2673–2682, Oct. 2010, doi: 10.1109/TPEL.2010.2050496.
[18] S. Cheng and T. G. Habetler, "Using only the DC current information to detect stator turn faults in automotive claw-pole generators," *IEEE Trans. Ind. Electron.*, vol. 60, no. 8, pp. 3462–3471, Aug. 2013, doi: 10.1109/TIE.2012.2205353.
[19] Y. Fan, C. Li, W. Zhu, X. Zhang, L. Zhang, and M. Cheng, "Stator winding interturn short-circuit faults severity detection controlled by OW-SVPWM without CMV of a five-phase FTFSCW-IPM," *IEEE Trans. Ind. Appl.*, vol. 53, no. 1, pp. 194–202, Jan./Feb. 2017, doi: 10.1109/TIA.2016.2609848.
[20] S. Wang, Y. Sun, Z. Huang, and S. Mu, "Analysis of stator internal phase-to-phase short circuit in the 12-Phase synchronous generator with rectifier-load system," *IEEE Trans. Energy Convers.*, vol. 33, no. 1, pp. 299–311, Mar. 2018.
[21] Y. Sun, S. Wang, W. Du, and S. Mu, "Analysis of armature inter-turn fault in the multiphase synchronous generator-rectifier system," *IET Electric Power Appl.*, vol. 13, no. 7, pp. 871–880, Jul. 2019.
[22] L. Hao et al., "Diagnosis of rotor winding short-circuit fault in multi-phase annular brushless exciter through stator field current harmonics," *IEEE Trans. Energy Convers.*, vol. 36, no. 3, pp. 1808–1817, Sep. 2021.
[23] Y. Wu, B. Cai, and Q. Ma, "An online diagnostic method for rotary diode open-circuit faults in brushless exciters," *IEEE Trans. Energy Convers.*, vol. 33, no. 4, pp. 1677–1685, Dec. 2018.
[24] H. K. Bui, N. Bracikowski, M. Hecquet, K. -L. Zappellini, and J. -P. Ducreux, "Simulation of a large power brushless synchronous generator (BLSG) with a rotating rectifier by a reluctance network for fault analysis and diagnosis," *IEEE Trans. Ind. Appl.*, vol. 53, no. 5, pp. 4327–4337, Sep./Oct. 2017, doi: 10.1109/TIA.2017.2701789.
[25] C. Di, I. Petrov, J. J. Pyrhönen, and J. Chen, "Accelerating the time-stepping finite-element analysis of induction machines in transient-magnetic solutions," *IEEE Access*, vol. 7, pp. 122251–122260, 2019.
[26] W. Shanming, W. Xiangheng, L. Yixiang, S. Pengsheng, M. Weiming, and Z. Gaifan, "Steady-state performance of synchronous generators with AC and DC stator connections considering saturation," *IEEE Trans. Energy Convers* ., vol. 17, no. 2, pp. 176–182, Jun. 2002.
[27] S. Williams and I. R. Smith, "Rapid digital computation of 3-phase thyristor bridge circuits," *Proc. Inst. Elect. Engineers*, vol. 120, no. 7, pp. 791–795, Jul. 1973.
[28] X. H. Wang, S. L. Chen, W. J. Wang, Y. G. Sun, and L. Y. Xu, "A study of armature winding internal faults for turbogenerators," *IEEE Trans. Ind. Appl.*, vol. 38, no. 3, pp. 625–631, May/Jun. 2002.
[29] X. H. Wang, Y. G. Sun, B. Ouyang, W. J. Wang, Z. Q. Zhu, and D. Howe, "Transient behavior of salient-pole synchronous machines with internal stator winding faults," *IEE Proc. - Electric Power Appl.*, vol. 149, no. 2, pp. 143–151, Mar. 2002.
[30] J. D. Gao, L. Z. Zhang, and X. H. Wang, *AC Machine Systems*. Berlin, Germany: Springer, 2009.

Liangliang Hao (Member, IEEE) was born in Heilongjiang, China, in 1985. He received the B.S. degree in electrical engineering from Hunan University, Hunan, China, in 2007, and the Ph.D. degree in electric machine and its system from Tsinghua University, Beijing, China, in 2012.

Since 2014, he has been an Assistant Professor with the School of Electrical Engineering, Beijing Jiaotong University, Beijing, China. He has authored and coauthored more than 50 peer-reviewed journal and conference papers. His research interests include the interturn short circuits of field windings in large synchronous generator, and the analysis for electric machine and its system.

Jianlin Chen (Student_Member, IEEE) was born in Jiangxi, China, in 1994. He received the B.S. degree in electrical engineering from China University of Mining Technology, Jiangsu, China, in 2018. He is currently working toward the Ph.D. degree with the School of Electrical Engineering, Beijing Jiaotong University, Beijing, China.

His research interests include the fault diagnose, condition analysis, and monitoring of brushless exciter for synchronous generators.

Li He received the M.S. degree in electrical engineering and automation from Southeast University, Jiangsu, China, in 2005.

He is currently an Engineer with the Yangjiang Nuclear Power Co., Ltd., Yangjiang, China. His research interests include fault diagnosis and maintenance of electrical equipment.

Xianwen Duan received the M.S. degree in electrical engineering and automation from South China University of Technology, Guangzhou, China, in 1987.

From 2008 to 2012, he was employed by the Daya Bay Nuclear Power Operations and Management Co., Ltd., Shenzhen, China, as a Project Engineer. Since 2012, he has been a Lead Electrical Engineer with the China Nuclear Power Operations Co., Ltd., Shenzhen, China. His research interests include electric machine protection and condition monitoring.

Peng He was born in Liaoning, China, in 1988. He received the M.S. degree in electrical engineering and automation from Jilin University, Jilin, China, in 2011.

Since July 2011, he has been an Engineer with the Liaoning Hongyanhe Nuclear Power Co., Ltd., Liaoning, China. His research interests include power system operation and excitation control of synchronous generators.

Guang Wang received the B.S. and M.S. degrees in electrical engineering from Tsinghua University, Beijing, China, in 2002 and 2005, respectively.

He is currently a Project Engineer with the Generator-transformer Protection Department, Nanjing NR Electric Co., Ltd., Nanjing, China. His research interests include application of advanced control, measuring techniques to provide innovative and effective solutions to emerging challenges in control and diagnostics of large-scale condensers and pumped-storage generators.